

Atomic-scale characterization of the nucleation and growth of SnO₂ particles in oxidized CuSn alloys

M. Dubey, X. Sauvage,* F. Cuvilly, S. Jouen and B. Hannoyer

University of Rouen, Groupe de Physique des Matériaux, CNRS-UMR 6634, BP-12, 76801 Saint Etienne du Rouvray Cedex, France

Received 16 July 2012; revised 6 September 2012; accepted 10 September 2012

Available online 14 September 2012

The internal oxidation of Sn was investigated to understand the oxidation kinetics of monophasic CuSn alloys. SnO₂ particles were characterized by analytical transmission electron microscopy. The orientation relationship between SnO₂ and Cu was determined with a special emphasis on the atomic-scale structure of Cu/SnO₂ interfaces (misfit dislocations and chemical structure). Habit planes with a pure oxygen plane terminating the SnO₂ phase are greatly favored and large misfits promote the growth of plate-shaped precipitates.

© 2012 Acta Materialia Inc. Published by Elsevier Ltd. All rights reserved.

Keywords: Internal oxidation; Copper alloy; SnO₂; Orientation relationship (OR); TEM

At elevated temperatures (i.e. 500–800 °C), the oxidation of pure copper is characterized by the formation of a double oxide layer of Cu₂O and CuO [1–4], in a ratio that depends on the temperature [5] and pressure [6]. As Cu₂O is a metal-deficient oxide in which the lattice diffusion of copper ions is several orders of magnitude faster than oxygen diffusion, the rate of growth of the cuprous oxide sublayer is controlled by outward diffusion of copper cations via metal vacancies [7,8]. In the top CuO layer, there are no vacancies available for fast diffusion of reacting species and hence the growth rate remains very low as compared to Cu₂O [9,10]. The presence of impurities in copper plays a very important role on the oxidation mechanisms and kinetics. Zhu et al. suggested that impurities could explain the discrepancies in the literature data reported for the copper oxidation kinetics [11]. Impurities impede the lateral growth of both Cu₂O [11] and CuO grains [2,9]; this favors grain boundary diffusion of Cu, faster than lattice diffusion, and consequently leads to an increased oxidation rate. Alloying element in solid solution in the face-centered cubic (fcc)-Cu phase can also strongly affect the oxidation kinetics. Depending on the alloying element diffusivity in both the alloy and metal oxides, various scenarios are reported. For example, in the case of oxidized Cu–Si alloys, a continuous SiO₂ layer appears at the Cu/Cu₂O interface. This layer significantly reduces

the oxidation rate which is explained by the lower diffusion rate of copper ions in SiO₂ than in Cu₂O [12,13]. For other alloys, such as Cu–Ti [14] or Cu–Ni [15], internal oxidation of the alloying element was reported. The nucleation of oxide particles inside the matrix is promoted by the oxygen diffusion [14,16] and these particles can exhibit various shapes and sizes depending on misfits and interfacial energies [17,18]. Their influence on the overall oxidation rate of the alloys is, however, not fully understood and could be rather complex. The case of CuSn alloys is of particular interest because a small amount of Sn slows down the oxidation kinetic, thus this element has a protective effect against oxidation. Internal oxidation of Sn was reported in 3–13 wt.% Sn alloys oxidized in 1 atm O₂ [19] and in 8.2 wt.% alloy oxidized in 1 atm laboratory air [20]. This phenomenon is attributed to the relatively low mobility of Sn. However, depending on the concentration and oxidation temperature, SnO₂ particles are detected in an inner mixed oxide layer of Cu₂O and SnO₂ or accumulated close to the alloy/scale interface [19–22]. The aim of the present work was to clarify the exact role of tin in the oxidation kinetics of CuSn alloys with a special emphasis on the nucleation and growth of SnO₂ nanoparticles precipitated internally in the fcc-Cu matrix.

Two model monophasic CuSn alloys were prepared by cast melting (provided by KME Corporation), containing 4.2 and 8.2 wt.% Sn, respectively (Cu balance). In the following, they are referred as CuSn4 and CuSn8, respectively. Samples for oxidation experiments were cut

* Corresponding author. Tel.: +33 2 32 95 51 42; fax: +33 2 32 95 50 32.; e-mail: xavier.sauvage@univ-rouen.fr

in coupons approximately 15 mm × 10 mm × 0.8 mm in size and homogenized under vacuum ($\sim 5 \times 10^{-5}$ mbar) at 600 °C for 4 h. Then, they were mechanically polished and finally cleaned with isopropanol and dried before oxidation. Oxidations were performed under laboratory static air in a muffle furnace maintained at 600 °C ($\pm 2\%$) for 4 h. After such a treatment, samples typically exhibit external multilayered oxide scales on the surface and an internal oxidation zone as discussed in Ref. [20]. To characterize the internally oxidized area, Transmission electron microscopy (TEM) samples were prepared from the specimen cross-section by the site-specific focused ion beam (FIB) lift-out technique [23] in a cross-beam NVISION-40 Zeiss®. Samples were then observed in a probe corrected JEOL® ARM200F transmission electron microscope operated at 200 kV. Energy-filtered images were recorded using a Gatan® Imaging Filter (GIF Quantum). High-angle annular dark-field (HAADF) images were recorded in scanning mode (STEM) with a 0.1 nm probe having a convergence angle of 30 mrad. The collection angle on the HAADF detector was in the range of 50–180 mrad.

In the internal oxidation zone, the Sn in solid solution is oxidized, giving rise to a two-phase mixture formed

from fcc-Cu matrix and a significant volume fraction of SnO₂. The number density of SnO₂ particle is rather low, and these particles are plate shaped as observed in the internal oxidation zone of the CuSn8 alloy (Fig. 1a). The thickness of these platelets is in the range of 10–50 nm, the length up to few micrometers and the width in the range of 50–100 nm (not shown here). There is a large distribution in the inter-plate spacing, from 100 to 500 nm. Energy-filtered (EF) TEM confirms that these platelets are embedded in the Cu matrix and are rich in Sn and O (Fig. 1a, inset). Furthermore, using electron diffraction, the crystallographic structure of the internal oxide platelets was identified; it matches the expected rutile structure of SnO₂ [24]. A diffraction pattern was recorded in the [110] zone axis of the fcc-Cu (Fig. 1b), and it is interesting to note that it also fits the [1-10] zone axis of SnO₂. Obviously, platelets are elongated along the Cu [-1 1 0] and the SnO₂ [001] directions. Internal oxide particles were also characterized in STEM. Since the average atomic number in the SnO₂ structure is lower than that of Cu, oxide platelets appear dark on HAADF images as shown in Figure 2a. The internal oxidation front is clearly exhibited on this image where platelets are growing from the top left corner

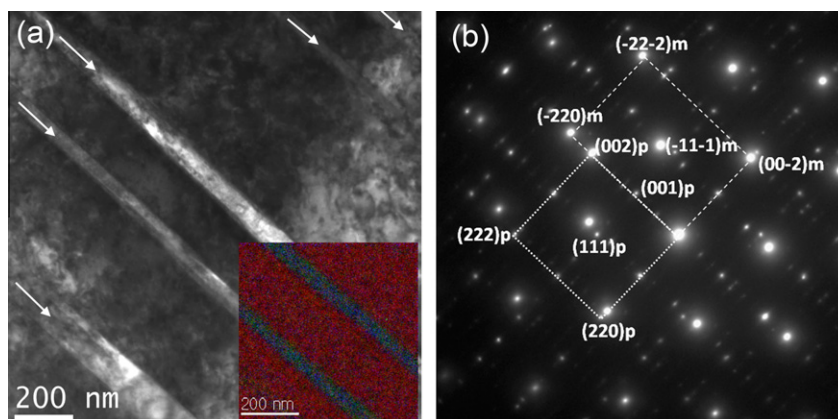


Figure 1. CuSn8 oxidized at 600 °C for 4 h. (a) BF-TEM image showing SnO₂ platelets (arrowed) within the Cu matrix; inset: EFTEM image (Cu, red; Sn, blue; O, green), confirming that the platelets are Sn and O rich (tin oxide). (b) Corresponding SAED pattern, spots are indexed: subscript **m** refers to the fcc-Cu matrix in the [110] zone axis and subscript **p** refers to the tetragonal SnO₂ oxide platelets in the [1-10] zone axis. (For interpretation of the references to colour in this figure legend, the reader is referred to the web version of this article.)

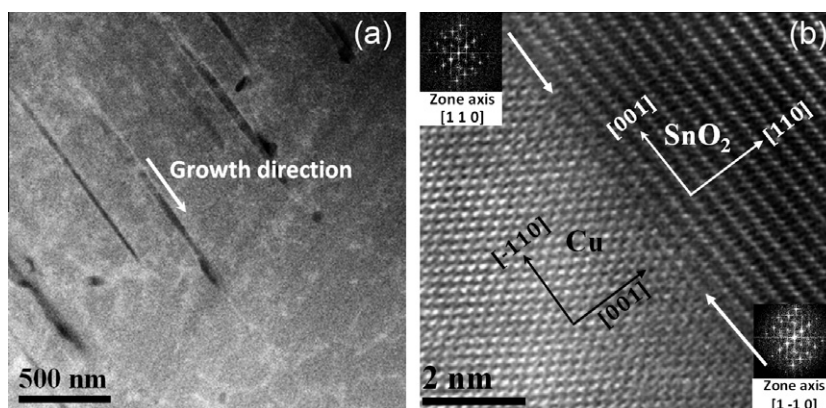


Figure 2. CuSn8 oxidized at 600 °C for 4 h. (a) Low-magnification HAADF-STEM images showing several parallel SnO₂ plates growing in the fcc-Cu matrix. (b) High-magnification HAADF-STEM filtered image showing the atomic structure of the Cu/SnO₂ interface in [1 1 0] fcc-Cu and [1-10] SnO₂ zone axes.

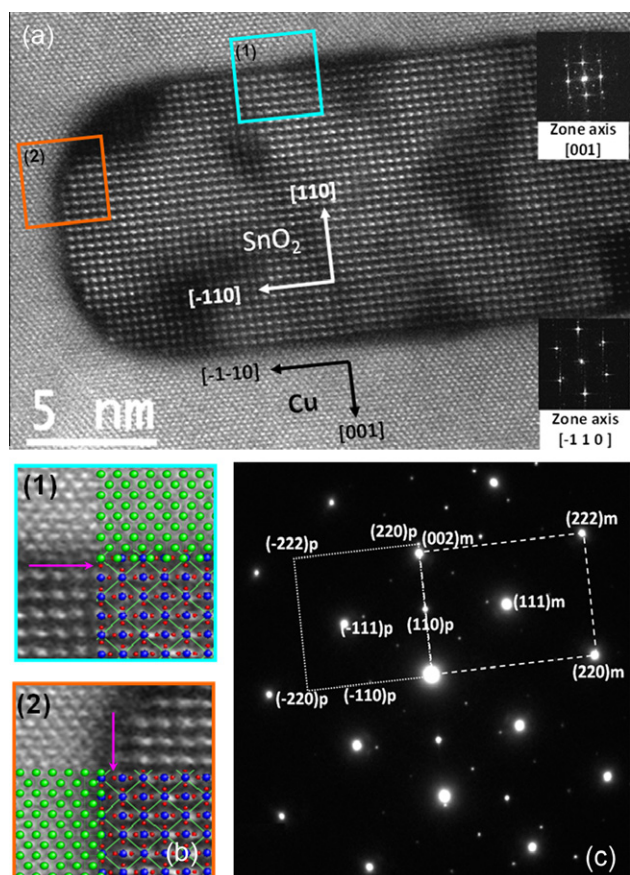


Figure 3. CuSn4 oxidized at 600 °C for 4 h. (a) HAADF HR-STEM image (unfiltered) of SnO₂ precipitate in [001] and [-1 1 0] fcc-Cu zone axes, where Sn- and Cu-rich columns are imaged. (b) Zooms of selected regions marked (1) and (2) in (a) showing the two Cu/SnO₂ interfaces with the overlap of Cu and SnO₂ crystal structures (Cu, green; Sn, blue; O, red). The arrows indicate the termination plane in the SnO₂ phase, being in both cases pure O. (c) SAED pattern giving the OR between the SnO₂ platelet *p* and the fcc-Cu matrix *m* of (a). (For interpretation of the references to colour in this figure legend, the reader is referred to the web version of this article.)

down to the bottom right. The high-resolution STEM-HAADF image (Fig. 2b) was obtained along the Cu [110] zone axis. On this image, only Cu- and Sn-rich atomic columns are brightly imaged. The Cu/SnO₂ interface (arrowed) appears edge-on and the orientation relationship (OR) between Cu and SnO₂ is thus given by: (002) Cu/(220) SnO₂ (habit planes) and [-110] Cu//[001] SnO₂.

It is interesting to note that the lattice mismatch along this interface, between (002) SnO₂ and (220) Cu planes, is positive (meaning that the matrix is in tension and the precipitate in compression) and relatively large, ~25%.

The microstructure in the internal oxide zone of the CuSn4 alloy looks very similar, i.e. there is a significant volume fraction of SnO₂ elongated plates. The diffraction pattern in Figure 3c shows that the OR between Cu and SnO₂ is similar to the OR found in the CuSn8 alloy. A platelet is imaged using high-resolution HAADF STEM in the [-1 1 0] zone axis of Cu, also corresponding to the [001] zone axis of SnO₂ (Fig. 3a). The

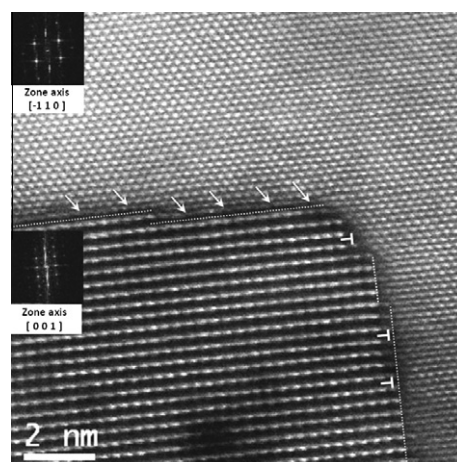


Figure 4. CuSn4 alloy oxidized at 600 °C for 4 h: HR-STEM HAADF unfiltered image showing the two habit planes between Cu and SnO₂ particles. Misfit dislocations are indicated by T-shaped symbols in the SnO₂ phase and by arrows in the Cu matrix. Interfaces and growth ledges are highlighted by dashed lines.

imaging is thus performed with the electron beam parallel to the growth direction of the plate. However, there are two different habit planes: (002) Cu for the long horizontal interface and (-2-20) Cu for the short vertical interface. For the first habit plane, the lattice mismatch between (-220) SnO₂ and (-2-20) Cu is very large (~31%) and positive, whilst for the second, the misfit between (220) SnO₂ and (002) Cu is negative and much smaller (~7%). These misfits are compensated by dislocations lying at the interface as underlined in Figure 4.

It is interesting to note that these large misfits do not inhibit the nucleation of the SnO₂ phase but surprisingly the thinnest dimension of SnO₂ plates does correspond to the lowest misfit. Two Sn oxides are reported in the literature, namely SnO and SnO₂. The free energy of formation of SnO₂ is much lower than that of SnO (-396 vs. -197 kJ mol⁻¹ at 600 °C [18]), so it was quite logical to observe only the SnO₂ phase even if in some cases the metastable SnO phase could be obtained [25]. In addition, the low number density of particles observed by TEM clearly indicates that the nucleation rate should be rather low. This is probably due to the large misfits creating large elastic distortions. Once nucleated, SnO₂ particles grow in the direction of the Sn-rich bulk, thus the internal oxidation kinetics is obviously mostly controlled by the growth and not the nucleation. SnO₂ particles are plate shaped, indicating that there is also some lateral growth. Indeed, while growing, these particles transform into elongated plates where the largest habit plane (002) Cu/(220) SnO₂ (marked (1) in Fig. 3a and b) combines the stronger misfits between the fcc-Cu matrix and the SnO₂ tetragonal phase (+25% and +31%) as demonstrated by our experimental data.

Metal-oxide interfaces have been investigated theoretically and experimentally (using high-resolution TEM) in various systems [26,27]. It has been shown that misfit dislocations along such interfaces are not defects like bulk dislocations but an integral part of the interface structure that is determined by the interaction between misfit and bonding. Thus, in the present case,

the growth of SnO_2 plates is also controlled by these interactions across the new interface that is created. HAADF HR-STEM images provide directly both chemical (Z contrast) and structural information. Overlapping the metal–oxide interfaces with Cu and SnO_2 crystal structures clearly exhibit along the two major habit planes (marked (1) and (2) in Fig. 3) a polar oxide interface terminated by a pure oxygen layer (red dots). Thus, the main difference between the two habits planes shown in Figure 3 is the misfit and it is rather surprising that the largest dimension of SnO_2 plates corresponds to the direction with the highest misfits and thus the highest elastic interaction. However, one should note that these misfits are largely positive, building up some tensile stresses in the copper matrix. Since the growth of SnO_2 particles requires some significant volume expansion (about 7% for CuSn4 and about 13% for CuSn8), and even if part of it is probably compensated by the outward diffusion of copper, this may favor a growth with some preferred habit planes leading to a compressive state in the SnO_2 particles.

In conclusion, large misfits between the tetragonal SnO_2 and the fcc-Cu phases give rise to a low nucleation rate. In combination with the tin gradient that builds up during the internal oxidation process, this lead to the formation of plate-shaped SnO_2 particles. The kinetics of internal oxidation is controlled by the growth of these plates. No significant differences were observed for the two alloys considered (CuSn4 and CuSn8). HR-STEM HAADF images directly show that polar oxide interface planes terminating by a pure oxygen plane are favored. However, elastic stresses also play an important role. Indeed, the elongation of the SnO_2 particles is promoted along directions where misfits lead to a tensile state in the matrix to compensate the volume expansion required for the internal oxidation of Sn. This feature promotes the plate-shaped growth of SnO_2 .

Authors would like to thank the Region Haute Normandie for the financial support of this work (research grant attributed to M.D.). M.D. would also like to thank N. Masquelier for fruitful discussions.

- [1] V. Prisedsky, V. Vinogradov, J. Solid State Chem. 177 (2004) 4258.
- [2] Y. Zhu, K. Mimura, M. Isshiki, Oxid. Met. 61 (2004) 293.

- [3] D.W. Bridges, J.P. Baur, G.S. Baur, W. Margin Fassell, J. Electrochem. Soc. 103 (1956) 475.
- [4] G. Wallwork, W. Smeltzer, Corros. Sci. 9 (1969) 561.
- [5] G. Garnaud, Oxid. Met. 11 (1977) 127.
- [6] J. Park, K. Natesan, Oxid. Met. 39 (1993) 411.
- [7] E. Iguchi, K. Yajima, Y. Saito, Trans. Jpn. Inst. Met. 14 (1973) 423.
- [8] S. Mrowec, A. Stoklosa, Oxid. Met. 3 (1971) 291.
- [9] Y. Zhu, K. Mimura, M. Isshiki, Corros. Sci. 47 (2005) 537.
- [10] Y. Zhu, K. Mimura, M. Isshiki, Oxid. Met. 59 (2003) 575.
- [11] Y. Zhu, K. Mimura, J.-W. Lim, M. Isshiki, Q. Jiang, Metall. Mater. Trans. A 37 (2006) 1231.
- [12] J. Kapteijn, S.A. Couperus, J.L. Meijering, Acta Metall. 10 (1969) 1311.
- [13] W. Tomlinson, J. Yates, Oxid. Met. 12 (1978) 323.
- [14] S. Wood, D. Adamonis, A. Guha, W.A. Soffa, G.H. Meier, Metall. Mater. Trans. A 6 (1975) 1793.
- [15] R. Haugsrud, P. Kofstad, Oxid. Met. 50 (1998) 189.
- [16] J. Megusar, G.H. Meier, Metall. Mater. Trans. A 7 (1976) 1133.
- [17] B.J. Kooi, J.T.M. De Hosson, Acta Mater. 48 (2000) 3687.
- [18] B.J. Kooi, H.B. Groen, J.T.M. De Hosson, Acta Mater. 46 (1998) 111.
- [19] F. Gesmundo, C. De Asmundis, S. Merlo, Werkst. Korros. 30 (1979) 114.
- [20] M. Dubey, S. Jouen, X. Sauvage, B. Hannoyer, Mater. High Temp. 28 (2011) 377.
- [21] C. De Asmundis, F. Gesmundo, P. Nanni, Werkst. Korros. 34 (1983) 95.
- [22] F. Mathis, M. Aucouturier, P. Trocellier, Explanation of Tin Role in the High Temperature Oxidation Resistance of Bronzes. Wiley-VCH Verlag GmbH & Co. KGaA, 2007, pp. 137–143. <http://dx.doi.org/10.1002/9783527610327.ch18>.
- [23] F.A. Stevie, C.B. Vartuli, L.A. Giannuzzi, T.L. Shofner, S.R. Brown, B. Rossie, F. Hillion, R.H. Mills, M. Antonell, R.B. Irwin, B.M. Purcell, Surf. Interf. Anal. 31 (2001) 345.
- [24] M. Batzill, U. Diebold, Prog. Surf. Sci. 79 (2005) 47.
- [25] H. Lorenz, Q. Zhao, S. Turner, O.I. Lebedev, G. Van Tendeloo, B. Klötzer, C. Rameshan, S. Penner, Mater. Chem. Phys. 122 (2010) 623.
- [26] J.T.M. De Hosson, H.B. Groen, B.J. Kooi, V. Vitek, Acta Mater. 47 (1999) 4077.
- [27] W.P. Vellinga, J.T.M. De Hosson, V. Vitek, Acta Mater. 45 (1997) 1525.